J. Jpn. Soc. Powder Powder Metallurgy, **72** (2025) 10-15
https://doi.org/10.2497/jjspm.24-00037

Paper

Preparation, Oxidation Resistance and Electrical Resistivity of Polycrystalline Single Phase RuB_2 Material by Arc-melt Method

Kunio YUBUTA[1], Kaoru KOUZU[2]*, Akiko NOMURA[3], Shigeru OKADA[2,4], Takeshi HAGIWARA[4], Toru KAWAMATA[3], Kazumasa SUGIYAMA[3], Yasukazu MURAKAMI[1], Toetsu SHISHIDO[3], Akira YOSHIKAWA[3] and Takao MORI[5,6]

[1]Dept. of Applied Quantum Physics and Nuclear Engineering, Kyushu University, 744 Motooka, Nishi-ku, Fukuoka 819-0395, Japan.
[2]Dept. of Science and Engineering, Kokushikan University, 4-28-1 Setagaya, Setagaya-ku, Tokyo 154-8515, Japan.
[3]Institute for Materials Research, Tohoku University, 2-1-1 Katahira, Aoba-ku, Sendai 980-8577, Japan.
[4]Research Institute for Engineering, Kanagawa University, 3-27-1 Rokkakubashi, Kanagawa-ku, Yokohama 221-8686, Japan.
[5]International Center for Young Scientists (ICYS), National Institute for Materials Science (NIMS), 1-1 Namiki, Tsukuba 305-0044, Japan.
[6]International Center for Materials Nanoarchitectonics (WPI-MANA), National Institute for Materials Science (NIMS), 1-1 Namiki, Tsukuba 305-0044, Japan.

Received June 1, 2024; Accepted July 16, 2024; J-STAGE Advance Published date: July 31, 2024

ABSTRACT

A single-phase RuB_2 (orthorhombic, space group *Pmmn*) polycrystalline material was successfully synthesized by the arc melting method. The condition for obtaining a single-phase RuB_2 material is dependent on the composition and form of the raw materials, namely using the composition of atomic ratio Ru:B = 1:2.1 and using granules Ru and B as the raw materials. The lattice constants of a single-phase RuB_2 obtained by the arc melt method are a = 4.645(1), b = 2.865(1), c = 4.046(1) Å, V = 53.8(1) Å^3. A thermogravimetric-differential thermal analysis (TG-DTA) for RuB_2 was carried out from room temperature to 1473 K. The oxidation reaction of RuB_2 begins at about 570 K, and the weight gain rate of final oxidation is 29%. Interestingly, the RuB_2 material was found to have a significantly lower oxidation resistance than Ru metal. The product after heating up to 1473 K in air atmosphere is a mixture of $RuB_{1.1}$ (RuB) and Ru phases, and B_2O_3 which is probably produced in an amorphous state. The values for electrical resistivity of RuB_2 are in the ranges from 23.3×10^{-3} to 102.2×10^{-3} Ω·cm.

KEY WORDS

arc-melt method, single RuB_2 polycrystalline material, lattice constant, oxidation reaction heated in air, electrical resistivity

1 Introduction

In the binary ruthenium (Ru)-boron (B) system the intermediate phases Ru_7B_3 (hexagonal, space group $P6_3/mc$), $Ru_{11}B_8$ (orthorhombic, space group *Pbam*), RuB ($RuB_{1.1}$) (hexagonal, space group $P\bar{6}m2$), Ru_2B_3 (hexagonal, space group $P6_3/mmc$), Ru_2B_5 (hexagonal, space group $P6_3/mmc$), RuB_2 (orthorhombic, space group *Pmmn*) have been reported[1,2]. Among these, the crystal system of $Ru_{11}B_8$ is orthorhombic, and $Ru_{11}B_8$ and Ru_2B_5 do not exist in the equilibrium phase diagram of Ru-B[3,4]. Recently, Zhen Gao et al.[5] report a single-phase RuB_4 powder (space group *Pmma*). From the phase diagram of the Ru-B system, it has been reported that the B atom of RuB is a solid solution in the composition range of ~49 to 53%, i.e., the RuB has a nonstoichiometry[1]. The RuB phase in this study is indicated as $RuB_{1.1}$. There are no detailed reports on the synthesis and physicochemical properties of RuB_2. This is because RuB_2 is difficult to obtain as a single-phase polycrystalline or single crystal, as the RuB_2 is an incongruent melting (a decomposition meltable) compound. The authors have previously prepared metal borides by high-temperature metal melt or arc melt methods to obtain metal diborides or ternary metal borides or solid solution metal borides[6-20]. In addition, in recent years, the metal diborides attract considerable attentions from researchers due to the superconductivity, magnetism and other intriguing physical properties[21-23]. For the Ru-B binary system, the phase diagram and the crystal structure and lattice constants of each phase are known[1-3]. On the other hand, the shapes of the single crystals in the Ru-B binary system are unknown. The Ru-B compounds have reported microhardness values. The hardness values were determined 22.2 GPa for RuB_2, 14.9 GPa for Ru_2B_3, 13.8 GPa for $RuB_{1.1}$ (RuB), 12.8 GPa for $Ru_{11}B_8$, and 11.1 GPa for Ru_7B_3[4], respectively. From these, it can be observed that boron-rich ruthenium boride tends to have the high hardness values.

* Corresponding author, E-mail: kouzu@kokushikan.ac.jp

Recently, Ru-B system compounds are considered promising as electrocatalytic active materials[24,25], and research is being actively conducted. A single-phase RuB_2 powder is synthesized using the CVD (chemical vapor deposition)[24] or molten salt assistance[25], and RuB_2 was synthesized after heating via molten salt (mixed crystal of KCl and LiCl) using RuO_2 and KBH_4 as starting materials[26]. However, there are few reports on the physicochemical properties of large RuB_2 crystals. In addition, physicochemical properties such as oxidation resistance and electrical resistivity of RuB_2 are unclear in experimental reports. Therefore, the authors decided to investigate the single crystal growth of RuB_2 and its characteristics. Unfortunately, the growth of RuB_2 single crystals of the desired size has not been realized so far. Although it was considered difficult to produce RuB_2 by directly synthesizing Ru and B using Ru and B as starting materials, the authors succeeded in obtaining a polycrystalline of RuB_2 single-phase by the arc melt reaction method. RuB_2 was investigated for oxidation behavior by heating in air using the TG-DTA method. In addition, the electrical resistivity of the RuB_2 polycrystalline was measured, and compared with the electrical resistivity of other two-component borides.

The crystal structure of RuB_2 is shown in Fig. 1. From this, the six-membered ring layers formed by the boron atom, and by the Ru atom are undulated, and form the similar layered structure of the AlB_2-type structure (hexagonal, space group *P*6/*mmm*) (Fig. 1-(a))[20,21]. In the AlB_2-type structure, the Al atom is located at the center of the six-membered ring formed by boron when viewed from the *c*-axis, on the other hand, in the RuB_2-type structure, the Ru atom is shifted to the site on the flat boron-boron bonding from the center of the boat-like six-membered boron ring along the *b*-axis and exhibits the stacking sequence *AA* perpendicular to the *c*-axis (Fig. 1-(b) and (c)). In addition, a deformed two-dimensional hexagonal boron sheets in the RuB_2 structure are corrugated along the *c*-axis. The crystal structure of the RuB_2 is similar to OsB_2 (orthorhombic, space group *Pmmn*)[4], but differs from MoB_2 (Mo_2B_{5-x}) (trigonal, space group $R\bar{3}m$)[21,23,27] and WB_2 (W_2B_{5-x}) (hexagonal, space group *P*6/*mmc*)[21,28,29].

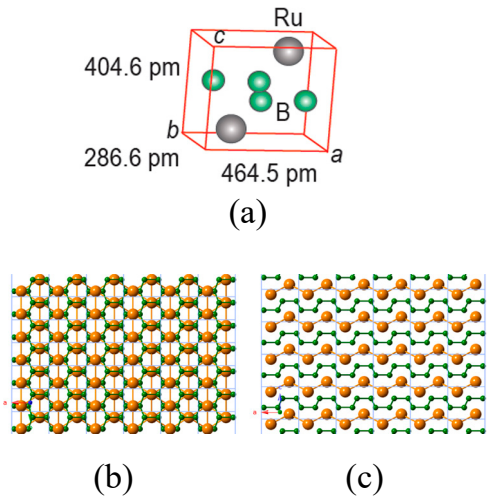

Fig. 1 Crystal structure of RuB_2.
(a): Three-dimensional structure of RuB_2, Projection from (b) the *c*- and (c) *b*-axes.
Large spherical: Ru, small spherical: B

2 Experimental details

The starting materials were metal ruthenium (Ru①) (Furuya Metal Co. 99.99% purity) powder, crystalline boron (B①) (Rare Metallic Co. purity 99.5%, 100 mesh or less) powder or granular crystalline B (B②) (High Purity Chemical Co. purity 99.5%, 3~7 mm granular) and Ru② (Ru① powder was arc-melted to produce by the button shape). An arc melting furnace was used to synthesize RuB_2. The arc melting furnace (ACM-01 type, DAIAVAC Co., Japan)[13] was used. After vacuuming the inside of the furnace to 2×10^{-5} Pa, it was replaced with high-purity Ar atmosphere, and an arc melting reaction was performed under the conditions of the voltage of 20~30 V and the current of 100~200 A. The compound was made into the button shape, and the button-shaped substance was turned over and melted again. This operation was performed five times to ensure homogeneity. Fig. 2 shows the button-shaped mass obtained by arc melting of the Ru-B system as the starting material, and the Ti metal getter was used to react with trace oxygen in the furnace. Thus, there is no impurity phase of oxides in the resulting arc melt. The button-like lump was cut into several pieces, cross-sectional observation was carried out using a scanning electron microscope (SEM) (JXA-8530F, JEOL Ltd., Japan). The button-shaped mass was pulverized, and the phases and lattice constants were measured using a powder X-ray diffractometer (XRD) (Ultima IV/SG, Rigaku Co., Japan). Composition analysis was performed using the field emission electron probe microanalyzer (FE-EPMA) (JXA-8530F, JEOL Ltd., Japan). The pulverized samples were inserted into a SiO_2 cell, and examined from room temperature to 1473 K by thermogravimetric-differential thermal analysis (TG-DTA) (TG-DTA 6300, Seiko Instrument Co., Japan) apparatus. Furthermore, after embedding the sample in resin and polishing, the electrical resistivity was measured at room temperature using the DC four-probe method, and the applied voltages were used at 10 mV, 100 mV and 1 V, respectively. The obtained electrical resistances were determined from the minimum and maximum values. The electrical resistance used KEITHLEY as the power supply and ESSTECH (ESS Tech

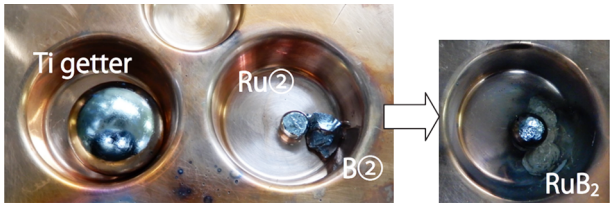

Fig. 2 Button-like lump obtained by arc-melting for starting materials of Ru-B system.

Co., Japan) by the compact prober system. The electrical resistivity (ρ) was obtained from the calculation of the following equation (1)[30].

$$\rho = 2\pi s(E/I) = 2\pi s(R). \quad (1)$$

Here, E: voltage, I: current, R: resistance, s: probe spacing (cm), π: pi.

3 Results and discussion

Table 1 shows the mixing conditions of the starting material, the yield obtained after arc melting, conditions for the formation of ruthenium borides. The XRD patterns obtained were shown in Fig. 3 together with RuB_2 (No. 01-079-8556) and Ru_2B_3 (No. 01-082-4437) ICDD cards[3]. Ru① and B① powders were used as raw materials, and arc melted at a compound atomic ratio Ru:B = 1:2 (run 1). In that case, the scattering of raw materials occurs during arc melting, and the yield after melting is 95.3%. The crystal phase arc melted sample was identified by the XRD. In addition to the RuB_2 phase, the Ru_2B_3 phase was confirmed as the second phase. Therefore, granules raw materials were used to prevent scattering of raw materials. The atomic ratio Ru:B = 1:2 (run 2) using granules Ru② and B② as raw materials had a yield of 99.6%, which was higher yield than that of run 1. From the XRD pattern of run 2, it was confirmed that the formation rate of the Ru_2B_3 phase was smaller than that of the RuB_2 phase. Therefore, when the atomic ratio of raw material B was increased by 5%, and arc melting was performed under the experimental conditions (atomic ratio Ru:B = 1:2.1) (run 3) of the mixing ratio of granules Ru② and B② as the starting material. As this result, a single-phase RuB_2 polycrystalline is obtained from the XRD pattern (run 3) and the yield is 99.8%.

The values for lattice constants of RuB_2 obtained are a = 4.645(1), b = 2.865(1), c = 4.046(1) Å, V = 53.8(1) Å^3, and the lattice constants of RuB_2 reported by Frotscher et al.[3] and V. Samsonov et al.[4] are a = 4.645, b = 2.865, c = 4.045 Å, V = 53.8 Å^3 and a = 4.6443, b = 2.8668, c = 4.0449 Å, V = 53.85 Å^3. These literature values are in good agreement with the authors values. From this, it can be inferred that RuB_2 synthesized by arc melting has a stoichiometric ratio.

The chemical properties were investigated by heating the sample in air using the TG-DTA apparatus. The results are shown in Fig. 4. Here, for comparison with RuB_2, RuO_2 (Furuya Metal Co., purity 99.9%) powder is shown together with Ru and B powders. From the TG curve, the oxidation initiation temperature of RuB_2 is about 570 K. In addition, the weight increase of RuB_2 after TG-DTA is 29%. Table 2 shows the temperature changes due to thermal behavior and weight increase in TG-DTA measurements using RuB_2, Ru, RuO_2 and B powders as samples. The XRD pattern after the oxidation reaction of RuB_2 is shown in Fig. 5 together with Ru and RuO_2 powders. As shown in the Fig. 5-(a), after heating $RuB_{1.1}$ and Ru phases were confirmed, B_2O_3 of the oxide of B

Table 1 Experimental results of arc melting.

	raw materials	Ru:B (atomic ratio)	yield (%)
run 1	Ru① + B①	1:2	95.3
run 2	Ru② + B②	1:2	99.6
run 3	Ru② + B②	1:2.1	99.8

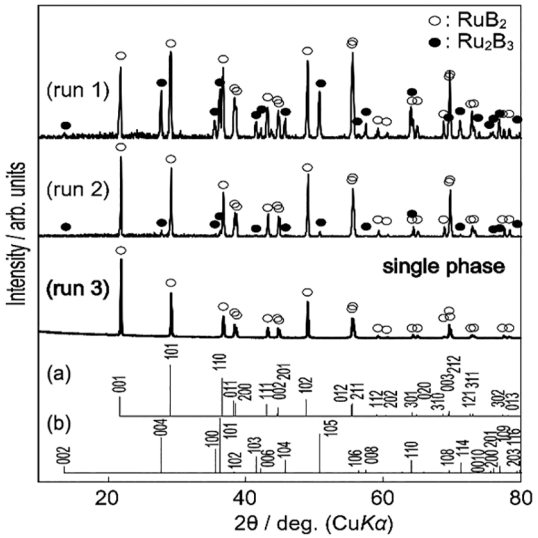

Fig. 3 Powder XRD patterns of samples synthesized by the arc melting method.
(a): RuB_2 (ICDD-01-079-8556)[3], (b): Ru_2B_3 (ICDD-01-082-4437)[3]

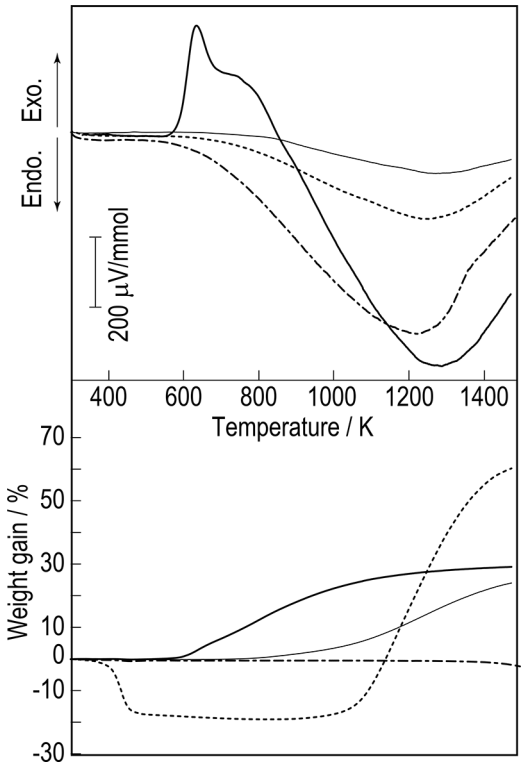

Fig. 4 The results for each TG-DTA curve using RuB_2, Ru, RuO_2 and B powders as samples.
Heating rate: 10 K/min.
——: RuB_2 (run 3), ——: Ru, ·····: B, -·-·-: RuO_2

Table 2 Temperature changes due to thermal behavior and weight increase in TG-DTA measurements using RuB_2, Ru, RuO_2 and B powders as samples.

samples	Oxidation onset temperature (K)	Weight gain at 1473 K (%)	Exothermal maximum (K)	Endothermal minimum (K)	Oxidized products
(a) RuB_2	570	29.2	633	1288	$RuB_{1.1}$ + Ru + RuO_2 + unknown
(b) Ru	770	24.1	-	1271	RuO_2 + Ru
(c) RuO_2	-	−1.8	-	1228	RuO_2
(d) B	1030	60.3	-	1252	adhesion to SiO_2 cell, uncollectable

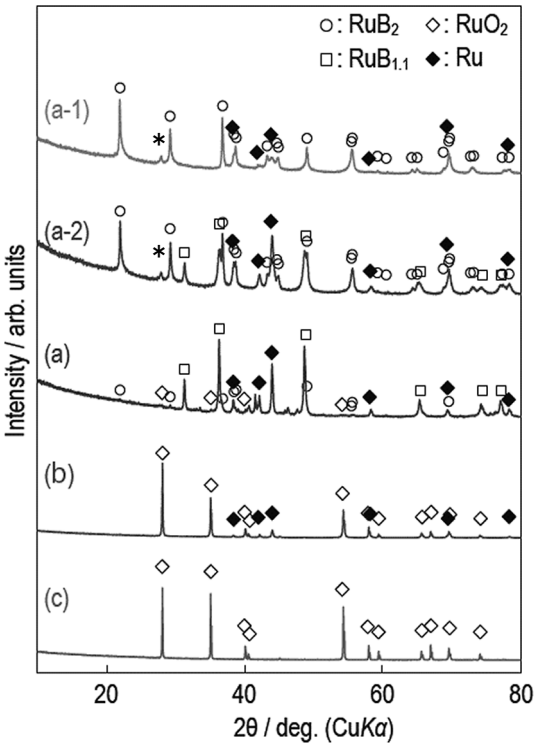

Fig. 5 Powder XRD patterns of samples after TG-DTA in air. (a) RuB_2, (b) Ru, (c) RuO_2: room temperature to 1473 K. (a-1): 600 K 1 h keep, (a-2): 700 K 1 h keep.
○: RuB_2 ◇: RuO_2 □: $RuB_{1.1}$ ◆: Ru, ∗: unknown

was not detected by the XRD pattern. The increase in the weight of the TG curve implies that B_2O_3 remains in the system in an amorphous state. In Fig. 5-(a), in addition to RuB_2, $RuB_{1.1}$, Ru, and RuO_2 phases are produced. In Fig. 5-(b), in addition to Ru, RuO_2 phase can be confirmed. In Fig. 5-(c), RuO_2 showed no change when RuO_2 was heated to 1473 K. In addition, the change in the maximum temperature of about 633 K according to the DTA curve of RuB_2 was examined, where the exothermic reaction of RuB_2 occurs. The XRD patterns of the compounds obtained by holding for 1 hour at heating temperatures of 600 K and 700 K were shown in Fig. 5-(a-1) and Fig. 5-(a-2), respectively. In the Fig. 5-(a-1), the RuB_2 and the Ru phases were identified, and in the Fig. 5-(a-2), Ru and $RuB_{1.1}$ phases were confirmed. However, a small unknown phase was present as indicated the reflection at $2\theta = 27.9°$. From the DTA curve, it was confirmed that at 633 K in the maximum exothermic reaction, Ru and $RuB_{1.1}$ (RuB) phases were formed. Thus, the oxidation reaction (2) of RuB_2 heated in air atmosphere is as follows:

$$3RuB_2 + 3O_2 \rightarrow 2RuB + Ru + 2B_2O_3. \quad (2)$$

Furthermore, the generated Ru is reacted to be RuO_2 at the heating temperature of 770 K or higher. When Ru powder was measured by TG-DTA curve in comparison with RuB_2, the oxidation initiation temperature was about 770 K. Interestingly, it can be seen that the RuB_2 material, with an oxidation initiation temperature of 570 K, has a lower oxidation resistance to being heated in air atmosphere than Ru metal.

After TG-DTA, RuB_2 was embedded in the resin, and observed with FE-EPMA apparatus. The results are shown as the microscope photographs in Fig. 6. It was difficult to polish the surface of the RuB_2 sample obtained by the arc melting method when conventional method of polishing were employed (Fig. 6-(A)). From the backscattered electron image (Fig. 6-(B)), it was observed that the shape of the crystal appeared clothed in a net-like shape on the crystal surface. The mixing ratios of boron (Fig. 6-(C)), oxygen (Fig. 6-(D)), and ruthenium (Fig. 6-(E)) were compared at each site by EDS mapping. There is a large amount of ruthenium in the reticular part and its vicinity that were observed brightly (white part) in Fig. 6-(B). On the other hand, Fig. 6-(B), the dark (gray area) observed part without the net has the flat plate or layered shape, indicating the presence of boron. This suggests that the abundance of lower atomic number boron has increased. The quantitative analysis of each site by EPMA suggested the presence of RuB_2 in the flat plate or layered part as shown in Fig. 6-(B). Consequently, it can be inferred that RuB_2 has a stoichiometric ratio.

Electrical resistivity was investigated as a representative physical property. The values for electrical resistivity of RuB_2 are in the ranges from 23.3×10^{-3} to 102.2×10^{-3} Ω·cm. The electrical resistivity of the two-component borides were reported to take various values, namely, at 5.2×10^{4}~9.0×10^{4} Ω·cm for $B_{12}P_2$ (p-type), 1.0 Ω·cm for B_4C[31], 0.1~10 Ω·cm for B_4C[32], 1.7×10^{13} Ω·cm for hBN, 1×10^{16} Ω·cm for cBN, 8.8×10^{-4} Ω·cm for $RhB_{\sim 1.1}$, 40×10^{-9} Ω·cm for TiB, 35×10^{-9} Ω·cm for VB, $57(\pm 8) \times 10^{-9}$ Ω·cm for MnB[4], 13×10^{-6} Ω·cm for ScB_2, 5.7×10^{-6} Ω·cm for TiB_2, 38×10^{-6} Ω·cm for VB_2, 39×10^{-6} Ω·cm for YB_2[33], 2×10^{-2} Ω·cm for BeB_2[4], 28.5×10^{-6} Ω·cm for YB_4, $24(\pm 12) \times 10^{-6}$ Ω·cm for LaB_4[4], 40×10^{-6} Ω·cm for YB_6, 20.7×10^{-5} Ω·cm

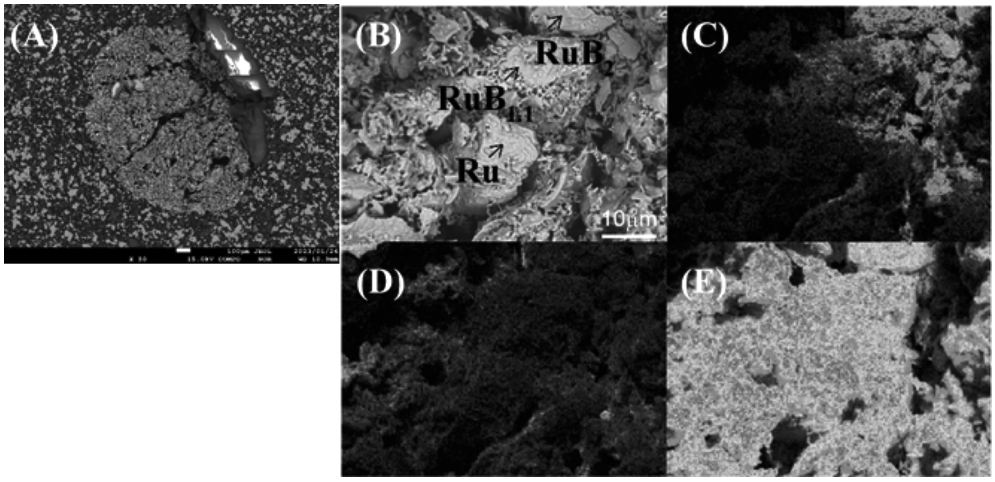

Fig. 6 BSE image and EDS mapping of RuB_2 after TG-DTA from room temperature to 1473 K.
(A): Overall view of sample embedded in resin
(B): (A) Enlarged view of Ru, $RuB_{1.1}$, and RuB_2 from the outside
(C): Boron concentration distribution in (B)
(D): Oxygen concentration distribution in (B)
(E): Ru concentration distribution in (B)

for SmB_6[4], 25.56 × 10^{-6} Ω·cm for DyB_{12}, 13.18 × 10^{-6} Ω·cm for HoB_{12}, 12.40 × 10^{-6} Ω·cm for ErB_{12}[33], respectively. The electrical resistivity of RuB_2 was found to be close to the values of $RhB_{\sim 1.1}$ and BeB_2. However, the values for the electrical resistivity of RuB_2 were higher than previously reported in the elemental-boron binary system of tetraborides or hexaborides or dodecaborides.

4 Conclusions

In the arc melting reaction method, the desired single-phase RuB_2 (orthorhombic, space group *Pmmn*) polycrystalline material was produced by devising the shape of the raw material and the amount of crystalline B to be prepared. As the result, the following conclusions were obtained.

1) The experimental conditions for obtaining a polycrystalline RuB_2 substance in a single phase are a mixed atomic ratio (Ru:B = 1:2.1) with granules Ru② and B② as starting materials. RuB_2 is a silver metallic color.
2) The lattice constants of a single-phase RuB_2 were a = 4.645(1), b = 2.865(1), c = 4.046(1) Å, V = 53.8(1) $Å^3$. It was in good agreement with the literature values.
3) The oxidation resistance of RuB_2 to heating in air was investigated by the TG-DTA method. After oxidation reaction of RuB_2, mainly, two phases of products were obtained as $RuB_{1.1}$ (RuB) and Ru phases. The generated Ru changes to RuO_2 at the heating temperature of about 770 K. In this reaction process, B_2O_3 phase could not detected by XRD suggesting that B_2O_3 may remain in the system for an amorphous state.
4) Quantitative analysis of FE-EPMA suggested the presence of RuB_2 with a stoichiometric ratio.
5) The values for electrical resistivity of RuB_2 are in the ranges from 23.3 × 10^{-3} to 102.2 × 10^{-3} Ω·cm.

Acknowledgments

For FE-EPMA measurements, we received the support of Mr. Narita, Technical Staff of the Institute for Materials Research, Tohoku University. In this experiment, we received the cooperation of the Cooperative Research and Development Center for Advanced Materials (CRDAM), Institute for Materials Research (IMR), Tohoku University. We would like to express our gratitude here. TM acknowledges support from JST Mirai JPMJMI19A1. KY gratefully acknowledges the support from JSPS KAKENHI (Grant No. JP23K04373). This study was conducted under the GIMRT Program of the Institute for Materials Research, Tohoku University (Proposal No. 202211-RDKGE-0008 and 202311-RDKGE-0001)

References

1) T. B. Massalski (ed.): Binary Alloy Phase Diagrams, Second Edition, Vol. 1, ASM International, (1990) 527-529. (W. Obrowski, Binary Alloy Phase Diagrams, II Ed. 1 (1990)).
2) R. B. Roof, et al.: J. Chem. Phys., **37** (1962) 1473-1476.
3) M. Frotscher, et al.: Z. Anorg. Allg. Chem., **636** (2010) 1783-1788.
4) G. V. Samsonov, I. M. Vinitskii: Refractory Compounds Handbook, NiSo Tsushinsha (RSS), (1976) 53-235.
5) Z. Gao, F. Ma, H. Wu, Y. Ge, Z. Zhu, Y. Liu, Y. Jiao, Z. Chen: J. Mater. Chem. A, **11** (2023) 3717-3724.
6) S. Okada, K. Kudou, K. Iizumi, K. Kudaka, I. Higashi, T. Lundström: J. Crystal Growth, **166** (1996) 429-435.
7) T. Shishido, J. Ye, S. Okada, K. Kudou, T. Sasaki, S. Ishida, T. Naka, M. Oku, I. Higashi, H. Kishi, H. Horiuchi, T. Fukuda: J. Alloys Compds., **309** (2000) 107-112.
8) S. Okada, K. Kudou, T. Tanaka, T. Shishido, V. N. Gurin, T. Lundström: J. Solid State Chem., **177** (2004) 547-550.

9) S. Okada, T. Tanaka, A. Sato, T. Shishido, K. Kudou, K. Nakajima, T. Lundström: J. Alloys Compds., **395** (2005) 231-235.
10) T. Mori, I. Kuzmych-Ianchuk, K. Yubuta, T. Shishido, S. Okada, K. Kudou, Y. Grin: J. Appl. Phys., **111**(7) (2012) 07E127 1-3.
11) T. Shishido, K. Yubuta, T. Mori, M. Tanaka, K. Kudou, S. Okada, A. Nomura, T. Sugawara, et al.: J. Flux Growth, **8**(1) (2013) 12-17.
12) K. Yubuta, T. Mori, A. Leithe-Jasper, H. Borrmann, Y. Grin, S. Okada, T. Shishido: J. Solid State Chem., **219** (2014) 274-279.
13) T. Yamasaki, K. Kouzu, A. Nomura, S. Okada, T. Shishido, K. Yubuta, A. Yoshikawa, T. Mori: Transactions of Kokushikan University, Faculty of Science and Engineering, **11** (2017) 49-53.
14) S. Okada, K. Kouzu, T. Yamasaki, T. Mori, Q. Guo, T. Shishido, K. Yubuta, G. Rogl, P. Rogl: Solid State Phenomena, **289** (2019) 65-70.
15) K. Kouzu, T. Yamasaki, S. Okada, T. Mori, Q. Guo, T. Shishido, K. Yubuta, A. Nomura, A. Yoshikawa, P. Rogl: Solid State Phenomena, **289** (2019) 120-126.
16) K. Kouzu, T. Yamasaki, S. Okada, T. Mori, Q. Guo, K. Yubuta, A. Nomura, T. Shishido, A. Yoshikawa, P. Rogl: J. Jpn. Soc. Powder Powder Metallurgy, **66** (2019) 525-529.
17) K. Yubuta, A. Nomura, K. Kouzu, T. Yamasaki, S. Okada, T. Mori, A. Yoshikawa, K. Sugiyama, T. Shishido: Solid State Sciences, **102** (2020) 106177 1-5.
18) T. Shishido, A. Nomura, T. Sugawara, S. Kurosawa, K. Yubuta, K. Kouzu, S. Okada, K. Hayashi, et al.: J. Flux Growth, **15**(1) (2021) 2-10.
19) K. Yubuta, A. Yasuhara, A. Nomura, T. Shishido, K. Sugiyama, K. Kouzu, S. Okada, T. Mori: Solid State Sciences, **142** (2023) 107243 1-7.
20) K. Kouzu, S. Okada, T. Hagiwara, A. Nomura, T. Shishido, A. Shishido, K. Yubuta, C. Bourgès, T. Mori: J. Jpn. Soc. Powder Powder Metallurgy, **70** (2023) 461-465.
21) K. Takagi, R. Uno, K. Kimura, et al.: Fundamentals and Applications of Boron, Borides and Related Materials, CMC Co. (2008) 49-203.
22) V. I. Matkovich (ed.): Boron and Refractory Borides, Springer-Verlin Heidelberg New York, (1977) 351-438.
23) S. Gabani, K. Flachbart, K. Siemensmeyer, T. Mori: J. Alloys Compds., **821** (2020) 153201 (21 pp).
24) X. Zou, L. Wang, X. Ai, H. Chen, X. Zou: J. Royal Soc. Chem., **56** (2020) 3061-3064.
25) D. Chen, J. Zhu, Z. Pu, S. Mu: Chem. Eur. J., **27** (2021) 12257-12271.
26) D. Chen, T. Liu, P. Wang, J. Zhao, C. Zhang, R. Cheng, W. Li, P. Ji, Z. Pu, S. Mu: ACS Energy Lett., **5** (2020) 2909-2915.
27) I. Higashi, Y. Takahashi, S. Okada: J. Less-Common Met., **123** (1986) 277-283.
28) T. Lundström: Ark. Kemi., **30** (1968) 115-119.
29) S. Okada, K. Kudou, T. Lundström: Jpn. J. Appl. Phys., **34**(1) (1995) 226-231.
30) jis.eomec.com/jish06021995.
31) Y. Kumashiro, H. Yoshizawa, K. Shirai: Jpn. J. Appl. Phys., **10** (1994) 166-168.
32) G. V. Samsonov, I. M. Vinitskii: Handbook of Refractory Compounds, IFI/Plenum, New York, (1980) 233-245.
33) Y. Paderno, V. Filippov, N. S. Shitsevalova: Pro. 11th Int. Symp. Boron, Borides and Related Compounds, Tsukuba 1993 JJAP Series, **10** (1994) 154-155.